ב"ה

Supporting Information for

Combining polarized low-frequency Raman with XRD to identify long-range interactions in a metal–organic pyrolysis precursor

Tal Ben Uliel,[=] Eliyahu M. Farber,[=] Hagit Aviv, Wowa Stroek, Marilena Farbinteanu, Yaakov R. Tischler,* David Eisenberg*

Experimental

Single crystal X-ray diffraction (SC-XRD). The synthesis of the MOCPs was described in detail elsewhere.[1,2] In brief, nitrilotriacetic acid was mixed with both the carbonate and the hydroxide of the respective alkaline earth metal (4:1 carbonate:oxide ratio, based on metal ion content), with the base added to deprotonate H_3NTA. Solving the structure by XRD reveals crystalline 3D coordination polymers, with the compositions of: $[MgNH(CH_2COO)_3(H_2O)_3]$,[3] $[CaNH(CH_2COO)_3(H_2O)_2]$, $[SrNH(CH_2COO)_3(H_2O)_{1.5}]$, and $[BaNH(CH_2COO)_3]$, named MgNTA, CaNTa, SrNTA and BaNTA, respectively. The water content in the crystals, determined by thermal gravimetric analysis, matches the values reported by Budkuley and Naik in 1998 for the corresponding powders.[4]

SrNTA and BaNTA were recrystallized over the course of 10–14 days from a saturated aqueous solution of each salt, connected to a vial with acetone without direct contact between the two liquids. MgNTA was recrystallized by slow evaporation of EtOH into a concentrated aqueous solution of MgNTA at 4 °C. Over the course of two week colourless crystalline twin needles were formed.[5] CaNTA was recrystallized by layering a concentrated aqueous solution of CaNTA with acetone at 4 °C. Over the weekend, colorless crystalline cubes were formed. The crystal data have been collected on a Rigaku R-AXIS RAPID II diffractometer using graphite monochromated Mo-Kα radiation (λ = 0.71075 A) and the ω-ϕ scan technique. The structures were solved by direct methods and refined anisotropically using a full-matrix least-squares method based on F2 with the SHELXL 97 program.[6,7] Non-hydrogen atoms were refined anisotropically. Hydrogen atoms were located and included at their calculated positions and they were refined by a riding model. For Sr and Ba, data collection was performed using monochromated Mo Kα radiation, λ = 0.71073 Å, using φ and ω scans to cover the Ewald sphere. Accurate cell parameters were obtained with the amount of indicated reflections. For Sr and Ba, the structure was solved using Olex2 with the olex2.solve1 structure solution program[8,9] using charge flipping and refined with the SHELXL refinement package[10] using least squares minimization. All non-hydrogen atoms were refined with anisotropic displacement parameters. The hydrogen atoms were refined isotropically on calculated positions using a riding model with their U_{iso} values constrained to 1.5 times the U_{eq} of their pivot atoms for terminal sp^3 carbon atoms and 1.2 times for all other carbon atoms. Simulations of the 4 crystal structures, atomic distances, and plane calculations were performed in the Mercury

software.[11] CCDC 1470252,[5] 1857232, 2054973 and 2054974 include all supplementary crystallographic data for this paper. These data can be obtained free of charge from the Cambridge Crystallographic Data Centre via www.ccdc.cam.ac.uk/data_request/cif.

Raman spectroscopy. All Raman measurements were taken using a lab-built micro-Raman setup. Samples were excited using a single-mode laser excitation of 532 nm and 20 mW of optical power, which was integrated into an upright microscope (Olympus, BXFM) for reflective geometry measurements. The output scattering from the sample, which contained both Rayleigh and Raman signals was routed into a specialized optical blocking filter system (ONDAX, XLFMICRO) consisting of three narrowband volume holographic notch filters to block laser light and intense Rayleigh scattering, with OD > 9 rejection ratio, from entering into the spectrometer. The output of the blocking filters was fiber-coupled into an imaging spectrometer (Princeton Instruments, SP-2500i), and measured using an acquisition time of 30 seconds and grating groove density of 1800 g mm^{-1}, with an electron-multiplying charge-coupled device camera (Princeton Instruments, Pro-EM: 1600^2).

Polarized LF-Raman. Three perpendicular faces of a macroscopic BaNTA single crystal were excited by the laser. The achromatic λ/2 plate with retardance accuracy of > λ/100 was located inside the ONDAX box. Four polarization directions at 45° to each other were measured for each of three crystal facets (see below), followed by choice of a pair of spectra obtained at right angles to each other.

Thermal gravimetric analysis. Thermal gravimetric analysis (TGA) coupled with differential scanning calorimetry (DSC) was performed in a Netzch Jupiter® STA 449F3 instrument, under argon flow (20 mL min^{-1}), at a heating rate of 10 °C min^{-1}.

Additional discussion of the single crystal structures

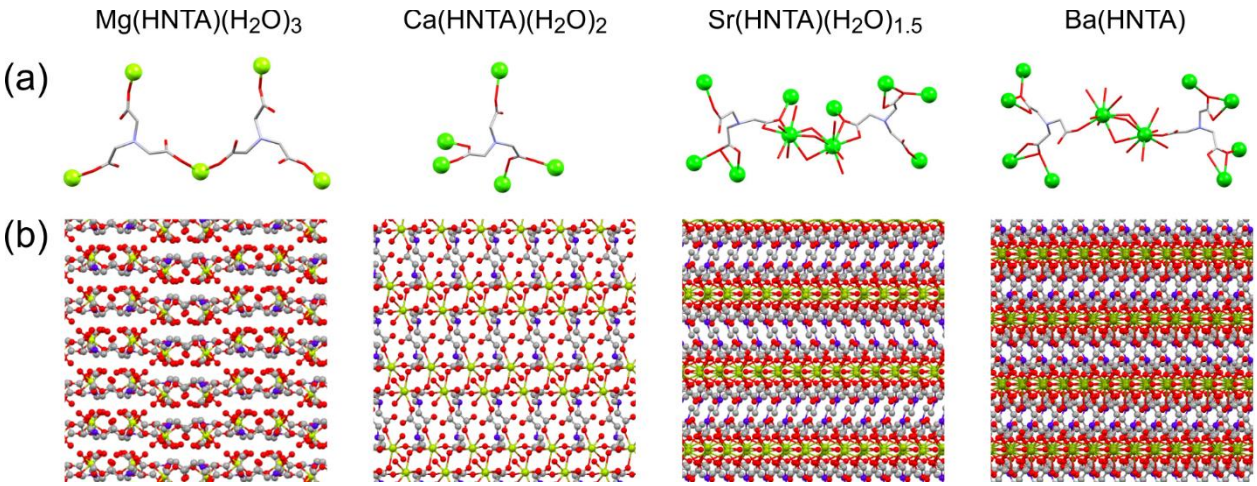

Figure S1. Single crystal structures of the four metal-organic coordination polymers. (a) Coordination mode of the Group 2 dications (green) to the nitrilotriacetate ligands (oxygen red, carbon grey, nitrogen blue, hydrogen atoms are omitted for clarity). (b) Molecular packing, viewed along the *c*, *b*, *a*, and *a* directions for MgNTA, CaNTA, SrNTA and BaNTA, respectively. Layers of M–O–M moieties (in green-red) are visible in SrNTA and BaNTA.

In MgNTA, each Mg^{2+} has an octahedral geometry, surrounded by three oxygens from three different $HNTA^{2-}$ ligands and three water molecules. The ligand nitrogen is protonated (not shown), and its carboxylate arms bind to three different Mg^{2+} ions. The metal ions and ligands are arranged in layers, linked by non-covalent interactions. In CaNTA, the Ca^{2+} ion has a distorted heptacoordinated geometry, coordinating to five oxygen atoms (from five different carboxylate groups) and two water molecules. Two carboxylate groups of each $HNTA^{2-}$ ligand are bridging two Ca^{2+} ions, whilst one carboxylate group is monodentate coordinated to a Ca^{2+} ion. In contrast, the building-block unit of the SrNTA structure is a dimer, in which the two Sr^{2+} ions are triply bridged by two carboxylate groups of two different $HNTA^{2-}$ ligands and one water molecule. A similar dimer unit is observed in the BaNTA crystal lattice, with pairs of Ba^{2+} ions triply bridged by carboxylate groups coming from two different $HNTA^{2-}$ ligands. The coordination of both Sr^{2+} and Ba^{2+} is completed by four oxygens from two different carboxylate groups of two independent $HNTA^{2-}$ ligands, and one oxygen from a water molecule. Thus, both the Sr^{2+} and Ba^{2+} ions have distorted nine-coordinated geometries. The variation in the coordination number and geometries reflects the increasing ionic radii from Mg^{2+} to Ba^{2+}, as well as the decreasing charge density of the ion. This trend is in agreement with similar trends observed for other alkaline-earth coordination polymers.[12–20]

Raman and LF-Raman of the four single crystal structures

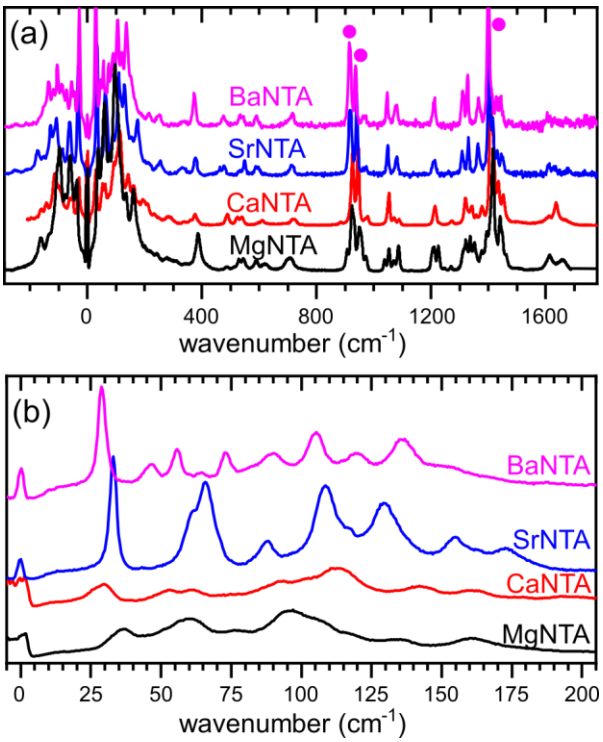

Figure S2. Raman spectra of the four alkaline-earth metal organic coordination polymers, in the (a) full frequency range, and (b) Stokes branch of the low frequency range. The dots mark peaks shifting gradually down the series, as discussed in the text.

The SrNTA and BaNTA Raman spectra are nearly identical, corresponding to the similarity in their single crystal XRD structures, and are better resolved than those of MgNTA and CaNTA, corroborating the observation that the former crystallize immediately while the latter are gooey solids. The Raman peaks at 915, 936 and 1399 cm^{-1} (BaNTA, marked by dots) shift consistently to higher vibrational energies down the series to MgNTA. However, since the connectivities are different, it is hard to derive meaningful information from the comparison.

Dehydration of the BaNTA crystal

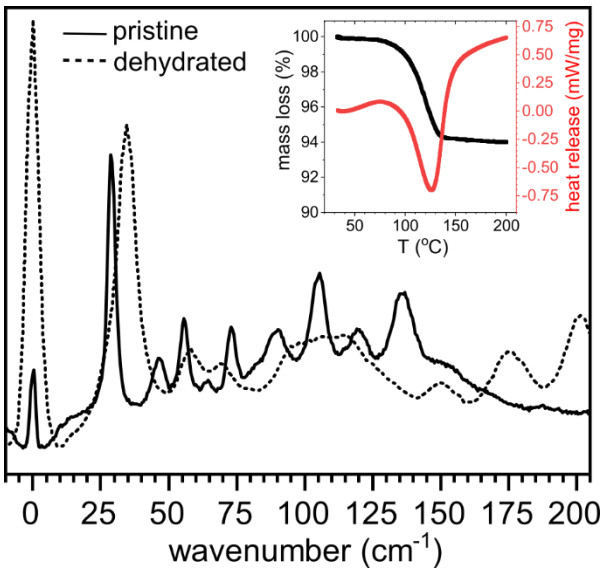

Figure S3. LF-Raman spectra of BaNTA in powder form before and after dehydration (heating to 200 °C). Inset: TGA-DSC characterization of the BaNTA powder (heating rate 1 °C/min), showing the loss of 1 water molecule per molecular unit around 126 °C.

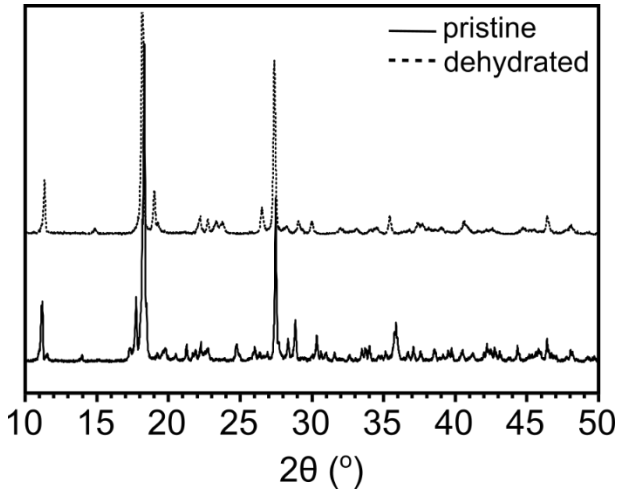

Figure S4. Powder XRD of BaNTA in powder form before and after dehydration (heating to 200 °C). The changes are minor, and consistent with dehydrations in the literature.[21,22]

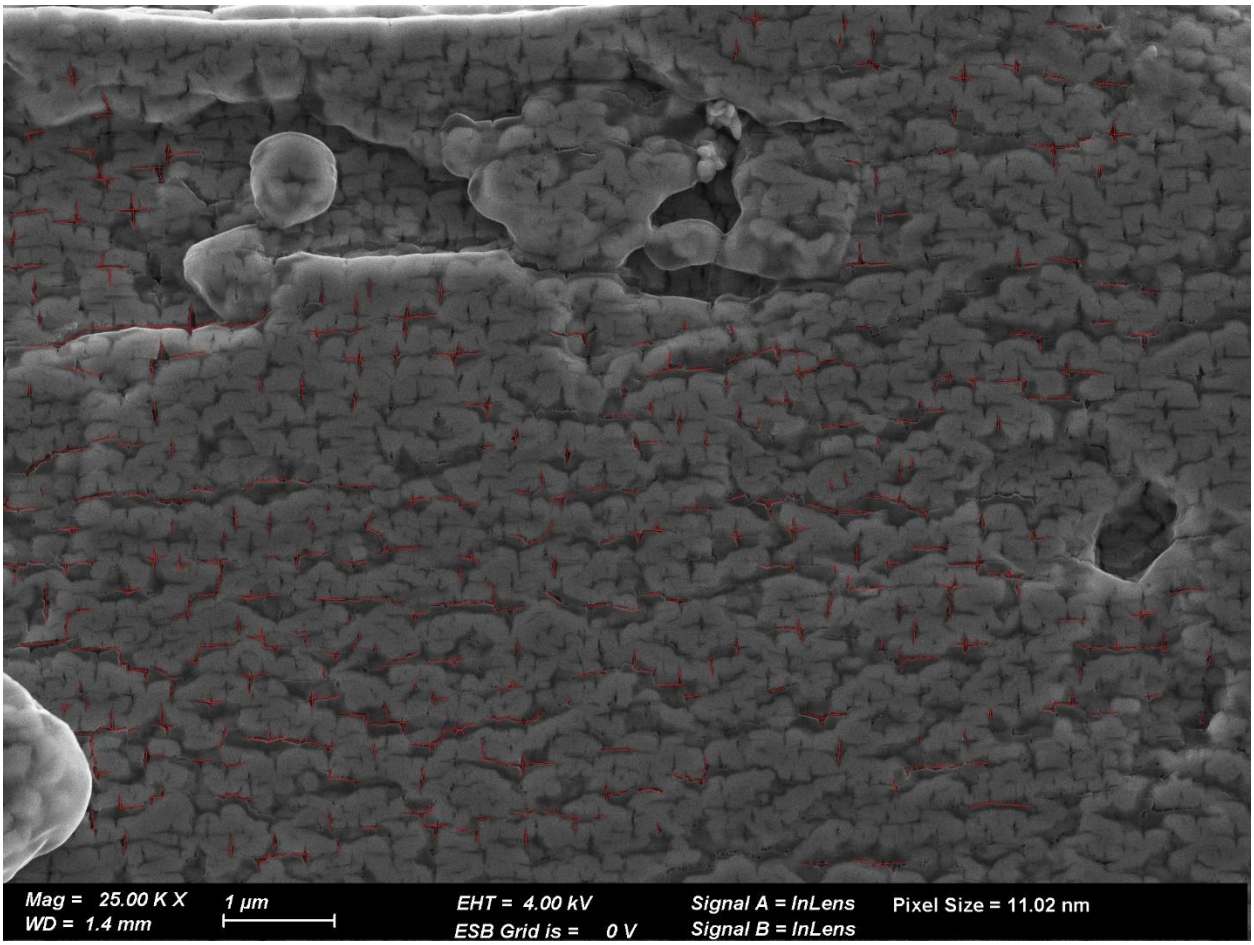

Figure S5. Full HRSEM micrograph of the BaNTA crystallite, with ~520 cracks marked for angle distribution analysis. The image edges are aligned with the crystallite edges.

References

1 D. Eisenberg, W. Stroek, N. J. Geels, C. S. Sandu, A. Heller, N. Yan and G. Rothenberg, *Chem. – Eur. J.*, 2016, **22**, 501–505.
2 E. M. Farber, K. Ojha, T. Y. Burshtein, L. Hasson and D. Eisenberg, *Mater. Adv.*, 2020, **1**, 20–33.
3 D. Eisenberg, W. Stroek, N. J. Geels, S. Tanase, M. Ferbinteanu, S. J. Teat, P. Mettraux, N. Yan and G. Rothenberg, *Phys. Chem. Chem. Phys.*, 2016, **18**, 20778–20783.
4 J. S. Budkuley and G. K. Naik, *Thermochim. Acta*, 1998, **320**, 115–120.
5 D. Eisenberg, W. Stroek, N. J. Geels, S. Tanase, M. Ferbinteanu, S. J. Teat, P. Mettraux, N. Yan and G. Rothenberg, *Phys. Chem. Chem. Phys.*, 2016, **18**, 20778–20783.
6 *Crystal Structure 4.0: Crystal Structure Analysis Package*, Rigaku Corporation, Tokyo, Japan, 2010.
7 G. M. Sheldrick, *Acta Crystallogr. A*, 2008, **64**, 112–122.
8 O. V. Dolomanov, L. J. Bourhis, R. J. Gildea, J. a. K. Howard and H. Puschmann, *J. Appl. Crystallogr.*, 2009, **42**, 339–341.
9 L. J. Bourhis, O. V. Dolomanov, R. J. Gildea, J. a. K. Howard and H. Puschmann, *Acta Crystallogr. Sect. Found. Adv.*, 2015, **71**, 59–75.
10 G. M. Sheldrick, *Acta Crystallogr. Sect. C Struct. Chem.*, 2015, **71**, 3–8.
11 C. F. Macrae, I. Sovago, S. J. Cottrell, P. T. A. Galek, P. McCabe, E. Pidcock, M. Platings, G. P. Shields, J. S. Stevens, M. Towler and P. A. Wood, *J. Appl. Crystallogr.*, 2020, **53**, 226–235.
12 Z.-T. Zhang, Q.-Y. Wang, W.-W. Li, Q.-H. Meng and X.-L. Zhang, *CrystEngComm*, 2012, **14**, 5042–5052.
13 J.-H. Wang, G.-M. Tang, T.-X. Qin, S.-C. Yan, Y.-T. Wang, Y.-Z. Cui and S. Weng Ng, *J. Solid State Chem.*, 2014, **219**, 55–66.
14 M. Usman, C.-H. Lee, D.-S. Hung, S.-F. Lee, C.-C. Wang, T.-T. Luo, L. Zhao, M.-K. Wu and K.-L. Lu, *J. Mater. Chem. C*, 2014, **2**, 3762–3768.
15 S. Du, C. Ji, X. Xin, M. Zhuang, X. Yu, J. Lu, Y. Lu and D. Sun, *J. Mol. Struct.*, 2017, **1130**, 565–572.
16 Y. Tang, A. Kourtellaris, A. J. Tasiopoulos, S. J. Teat, D. Dubbeldam, G. Rothenberg and S. Tanase, *Inorg. Chem. Front.*, 2018, **5**, 541–549.
17 Y. Tang, A. Cavaco Soares, M. Ferbinteanu, Y. Gao, G. Rothenberg and S. Tanase, *Dalton Trans.*, 2018, **47**, 10071–10079.
18 D. Rankine, T. D. Keene, C. J. Sumby and C. J. Doonan, *CrystEngComm*, 2013, **15**, 9722–9728.
19 X. Wang, M. Hu, J.-Y. Tian and C.-S. Liu, *CrystEngComm*, 2016, **18**, 2864–2872.
20 S.-C. Chen, F. Tian, K.-L. Huang, C.-P. Li, J. Zhong, M.-Y. He, Z.-H. Zhang, H.-N. Wang, M. Du and Q. Chen, *CrystEngComm*, 2014, **16**, 7673–7680.
21 A. Bērziņš and A. Actiņš, *CrystEngComm*, 2014, **16**, 3926–3934.
22 H. Oyama, T. Miyamoto, A. Sekine, I. Nugrahani and H. Uekusa, *Crystals*, 2021, **11**, 412.